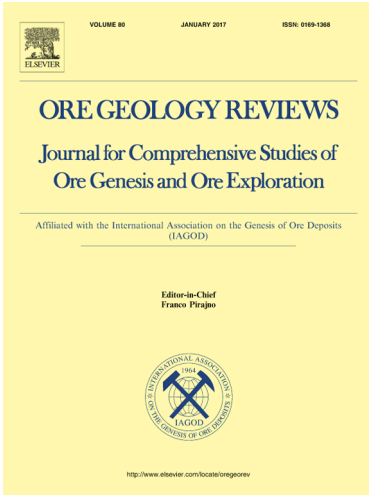

Characteristics and genesis of the Mnogovershinnoe gold-silver deposit, SE Russia

Vadim G. Khomich, Natalia G. Boriskina, Igor I. Fatyanov, M. Santosh

PII: S0169-1368(15)30147-5
DOI: http://dx.doi.org/10.1016/j.oregeorev.2017.01.017
Reference: OREGEO 2086

To appear in: *Ore Geology Reviews*

Received Date: 22 October 2015
Revised Date: 22 September 2016
Accepted Date: 17 January 2017

Please cite this article as: V.G. Khomich, N.G. Boriskina, I.I. Fatyanov, M. Santosh, Characteristics and genesis of the Mnogovershinnoe gold-silver deposit, SE Russia, *Ore Geology Reviews* (2017), doi: http://dx.doi.org/10.1016/j.oregeorev.2017.01.017

Characteristics and genesis of the Mnogovershinnoe gold-silver deposit, SE Russia

Vadim G. Khomich [a*, b], Natalia G. Boriskina [a, b], Igor I. Fatyanov [a], M. Santosh [c, d]

[a] Far East Geological Institute, Far East Branch of Russian Academy of Sciences, 159 Prospect 100 let Vladivostoku, Vladivostok 690022, Russia

[b] School of Engineering, Far Eastern Federal University, Russia
8 Suhanova St., Vladivostok 690950, Russia

[c] Department of Earth Sciences, University of Adelaide, SA 5005, Australia

[d] School of Earth Sciences and Resources, China University of Geosciences Beijing, 29 Xueyuan Road, Beijing 100083, China

*Corresponding author: Vadim G. Khomich. Tel.: + 79243305975, khomich79@mail.ru

Research Highlights

- The largest Au-Ag deposit in South East Russia
- Lateral and vertical zoning of mineral deposit
- Geodynamic model for the mineralization

Abstract

The Mnogovershinnoe ore deposit is part of the Bekchiul volcano-plutonic complex, located on the northern flank of the East-Sikhote-Alinsky belt in SE Russia. The complex was developed in two stages during the Senonian (Upper Cretaceous) and Paleocene-Eocene. The early stage is represented by a poorly differentiated andesite-granodiorite association and the late stage is marked by subalkaline monzodiorite-granite intrusions. The vein-metasomatic zones with Au-Ag mineralization are associated with magmatic units of the early stage and are crosscut by large dikes of the late stage. The deposit shows features of epithermal mineralization and a higher temperature overprint. The total ca. 1000 m zone of productive mineralization shows vertical zoning characterized by gold-sulfosalt-sulfide, gold-sulfide, then gold-telluride-sulfide, and telluride-sulfide, from bottom to top. The hydrothermal system of the deposit shows evidence for mixing between fluids derived from the volcano-plutonic units and meteoric water. The mineralization is inferred to have formed from the mixing between these fluids and by the fluctuations of fluid pressure in the system.

Key words: Gold; Silver; Zoning; Fluid mixing; Ore genesis.

1. Introduction

The Mnogovershinnoe gold-silver mineralization represents one of the largest precious metal deposits in southeast Russia. It was discovered in 1959 and has been exploited since 1991. Although not yet fully prospected, the reserve estimates at the beginning of exploitation shows more than 80 tonnes (2,822 million ounces) of gold (Yushmanov, 2014), which is expected to far exceed when more detailed investigations are completed.

In this study, we present a summary of the geological and ore mineralogical features of the mineralization in order to constrain ore genesis. We propose a new

50 interpretation for the spatial distribution of the ore deposit, located above a paleo-transform
51 fault at the convergence of the Paleo-Pacific Ocean and the Asian continent based on
52 seismic tomographic investigations. The deep-seated geodynamics has influenced the
53 scale of development of the magmatic, vein-metasomatic, and ore-bearing associations
54 and the formation of the mineralogical and geochemical zoning. The source, stages of the
55 formation of gold-bearing zones, and their relation to intrusions are evaluated.
56
57 **2. Geological and geophysical background**
58
59 The Mnogovershinnoe ore deposit is located in the Lower Amur ore district on the
60 northern flank of the East Sikhote-Alin marginal continental volcanic belt (Fig. 1).
61 Geophysicists interpret the thickness of the lithosphere in the region to be 100-120 km,
62 with a crustal thickness of 30-34 km (Didenko et al., 2010).
63 Based on previous studies, some workers consider that this deposit occurs on the
64 boundary of the Gorinsky and Lower Amursky terranes (Khanchuk, 1993), or at the
65 junction of the horst structure of the Amur-Okhotsk accretionary system, within the
66 Amursky rift-graben system (Utkin, 1999); the latter is supported by the density
67 heterogeneities at different depths (Khomich and Petrishchevsky, 2004; Petrishchevsky and
68 Yushmanov, 2014).
69 Correlation with global seismic tomographic investigations (Maruyama et al., 2007;
70 Zhao et al., 2010; Li and van der Hilst, 2010) indicates that the ore district (Fig. 2c) is
71 related to an extensive (> 2000 km) magmatic and metallogenic belt, above a major paleo-
72 transform fault (Khomich and Boriskina, 2014 a, b) (Fig. 2). The region lies above the
73 perimeter of a stagnant slab in the mantle transitional zone over which the world-class
74 Aldan, Balei, and Zhao-E gold deposits are located (Fig. 2; Khomich et al., 2014, 2015).
75 This is consistent with a proposal from geophysicists that the ore deposits are related to

asthenospheric upwelling, with a lower (3.20 g/cm^3) density of the lithospheric mantle, particularly characterized by a subvertical zone at depth (Didenko et al., 2010).

The Mnogovershinnoe ore deposit is part of the Bekchiul volcano-plutonic center (30x30 km) that formed during the Cretaceous-Paleogene period (Fig. 3). The interpretation of geophysical data shows a heterogeneous density distribution at a depth of ~100 km (Khomich and Petrishchevsky, 2004) and a laccolith-like form of a magma chamber. The laccolith thickness is ~5-6 km and decreases from the arch to flanks (Petrishchevsky, 1988). A notable feature of the volcano-plutonic center is the presence of a serpentinized ultramafic block (2x4 km), suggesting magma generation at depth (Fig.3). The volcano-plutonic center was formed in two stages: early Senonian (Upper Cretaceous) and late Paleocene-Eocene. In the first stage, poorly differentiated andesite-granodiorite association was formed, and the second stage is characterized by subalkaline differentiated monzo-granodiorite-granite association (Fatyanov and Khomich, 1997). The early stage of magmatic activity is related to the formation of thick vein-metasomatic zones with gold-silver mineralization whereas the late stage is represented by tourmaline-quartz veins without significant concentrations of precious metals.

3. Geology of the district

The ore district is located within the UI volcanic feature (10-14 km x 5-7 km, Fig. 4), represented by a graben-like depression in the western part of the volcano-plutonic center and bound in the north by a large latitudinal fault. The eastern and southern margins are marked by dislocations along the contact of the Bekchiul granitoid massif, and the western boundary is overlain by Neogene-Quaternary deposits. The basement is represented by the Upper Jurassic-Lower Cretaceous terrigenous deposits. The depression is filled with volcanic rocks of predominantly intermediate composition.

The sedimentary rocks underlying the volcanic facies are deformed into linear folds with northeast strike. The orientation of the folds that extend into the basement was inherited from the tectonic dislocations of the volcanic structure. It is assumed that the mineralized zones are aligned with the axial zones of anticlinal folds. Effusive-pyroclastic sediments, extrusive and subvolcanic bodies, located in the ore field, formed in the Late Cretaceous-Paleogene (Table 1, Fig. 3). Faults trending northeast and northwest are also common.

The northeast faults have steeply dipping dislocations, with displacements responsible for the block-faulted step-like structure of the district and an increase in thickness of the volcanic units with distance from the Bekchiul massif. Thick zones (up to 100 m) of extensive (to 5-7 km) veins with metasomatic halos and gold-silver mineralization are restricted to faults. These zones occur in volcanic rocks and extend into the basement to a depth of several hundred meters. The zones trace the system of dislocations that are responsible for the block structure of the district, with different degrees of erosion. The Vodorazdel'naya zone near the pluton is mostly eroded, whereas the Glavnaya zone is partly preserved and the Promezhutochnaya zone is little eroded. The Medvezh'ya zone, farthest from the pluton, about 3 km to the northwest, is largely unaffected by erosion, and has a halo of metasomatic alteration that formed above the ore zone (Fig. 4).

The *northwest faults* are oriented orthogonally to ore zones and offset these zones into several members with differential erosion. The central part is less eroded, whereas the flanks were more uplifted and underwent stronger erosion (Fig. 4). The northwestern system of dislocations controls tourmaline-quartz veins that do not contain significant concentrations of precious metals. Dikes, dike-like bodies and intrusions crosscut the volcanic structure and are also oriented northwest. The largest intrusion represented by granodiorite-porphyries divides the ore field into two domains. The major portion of the

ore-bearing zones occurs in the eastern part. Those in the western part are oriented both northeast and northwest.

4. Nature of ore-bearing veins

The mineralized zones occur as steeply dipping thick plate-like quartz bodies with lateral extents up to 100 m and are characterized by complex structure (Fig. 5). Around plate-like bodies, biotite-epidote-albite and sericite-chlorite-epidote-albite (biotite-free) facies have been identified (Fig 6). A summary of the salient features of mineralization is given below.

The volcano-plutonic complex at the center formed a dome-like edifice. Stress propagation occurred along both the earlier emplaced tectonic dislocations and orthogonal (across the strike of the former) faults with large fault-shift displacements. The dislocation fractures were almost synchronously healed with quartz-veins.

The altered halo at the top is several tens of meters thick, fringing the quartz veins. The lower part of altered zones is composed of light-grey quartz with various amounts K-feldspar and sericite. The upper part of the quartz body includes pyrite, chlorite, albite, sericite, and K-feldspar.

The veins are composed of fine-grained quartz with various amounts of adularia, sericite, and ore minerals (Fig. 7, 8). Adularia and sericite are usually dispersed in the quartz aggregate of the veins, and forms nest-like accumulations or are locally banded. Adularia is represented by two structural varieties: intermediate orthoclase (in the areas of brecciation) and high and intermediate microcline within the aureoles of the recrystallized quartz, fringing the brecciation areas (Fatyanov et al., 1989). Ore minerals include sulfides, sulfosalts, tellurides, and native gold (≤0.5-3 vol% of the vein), as thin and finely dispersed impregnations, and rarely as streak-like separations, or nest-like accumulations. A notable

feature of the ore mineralization is a wide spectrum of mineral species with low sulfide content of ores (Fig. 9). Among the sulfides, pyrite dominates, together with chalcopyrite (Fig. 7E), galena, and sphalerite, with sporadic pyrrhotite and arsenopyrite. Sulfosalts (grey ore, pearceite-polybasite) and tellurides (hessite, petzite) are present in subordinate amounts (Fig. 10). Tellurobismuthite, altaite, scheelite, and the following selenides occur rarely: naumannite, telluroselenides of silver, and galena-clausthalite (Fatyanov and Sapin, 1988). Native gold is distributed irregularly with fineness varying widely from 650 to 925.

In some areas, explosive breccias and cementation of fragments with quartz, adularia-quartz, and in some cases carbonate-quartz aggregates are also identified.

The carbonate fillings are represented by small lens-like carbonate bodies in the veins marked the latest stage of hydrothermal activity. In the Glavnaya zone, they are composed of dolomite and in Promezhutochnaya zone of calcite, usually Mn-bearing. The veins were cut along the northwestern faults by subalkaline granitoid intrusions, with skarn alteration of carbonates, now preserved in fragments. Carbonate precipitation may have continued after intrusion, as inferred from the presence of lenses of calcite with pyrite, galena, and sphalerite without evidence of skarn in the Glavnaya zone (Fig. 11).

The skarn-like Mn, Fe, and Mg-Fe metasomatic zone is related to late intrusion of subalkaline granitoid magmas and rejuvenation of the late-stage hydrothermal activity. In general, the skarn-like associations are usually developed at the contact of quartz veins with altered volcanic rocks.

The composition of the Mn-rich skarn zone is dominated by Mn-bearing wollastonite, bustamite and rare rhodonite (Fig. 7, 8). Garnet (spessartite, grossular-andradite) and Mn-bearing diopside and axinite occur in subordinate amounts. The Fe-rich altered unit is composed of grossular-andradite garnet (largely the andradite component), pyroxene (diopside-salite), and magnetite. Amphibole (tremolite-actinolite series), epidote, quartz, calcite, and hematite are present in variable amounts locally. Pyroxenes (diopside,

diopside-salite), amphiboles (tremolite, actinolite), epidote, serpentine, and magnetite occur in the Mg-Fe metasomatic domain.

The ore-forming associations of the skarn-altered zones do not show mineral diversity. In the area of replacement of Mn carbonates by skarn there are related galena, iron-free sphalerite (cleiophane), and locally gold (820-890 fineness). In the Fe-rich alteration, oxides (magnetite, locally hematite) and sulfides (pyrite and chalcopyrite) are common. In the Mg-Fe alteration zone, in addition to the dominance of magnetite and pyrite, the high-fineness gold (93.6%) and tellurobismuthite occur.

The contact-metamorphosed vein-related alteration is exposed in the aureole of the late-stage intrusions. At the contact with monzogranodiorites, dense fine-grained quartz is transformed into semi-transparent coarse-grained (up to 5-7 mm) quartz aggregate containing emulsion-like coatings of K-feldspar. With distance from the contact, this quartz gradually transforms to fine-grained sugary aggregates. This zone also shows the formation of hornfels in hydrothermally altered rocks along with the development of a biotite-amphibole-K-feldspar association.

Superimposed tourmaline-quartz also occurs in the vein zones, represented by quartz with variable quantities of tourmaline and rare feldspar. Usually the streaks and veinlets show a northwest orientation orthogonal to the strike of ore zones.

Among the various zones described above, the quartz veins are dominant and others comprise only 3-7 % of the total volume.

5. Lateral zoning of vein-related alteration

The genesis of Mnogovershinnoe deposit is complex, with combined features of epithermal deposits overprinted by higher temperature mineralization. Geochemical investigations indicate vertical zoning in the distribution of Au (Fig. 12) and others ore-

206 forming elements, characterized by Mo, Sn, and locally W, Cu, Ni, and Co at deeper
207 levels, with change at shallower levels to anomalous Pb, Zn, Ag, and Au (Table 2).

208 In the individual deposits of the vein zones, the lower and middle levels are
209 characterized by maximum thickness of the quartz vein and alteration halo (Fig. 5, 6). The
210 thickness decreases at shallower levels, then splits into several vein-like bodies, and
211 finally into a series of veins. Significant decrease in thickness also occurs downward from
212 of the main ore zone.

213 The zonation also occurs in the cover of the hydrothermally altered rocks around
214 the quartz veins (Fatyanov and Khomich, 1989).

215 The alteration halos around the quartz veins also show lateral zoning (Fig. 6). Two
216 zones are distinct: an inner zone composed of quartz with variable quantities of sericite
217 and K-feldspar and an outer zone with sericite, K-feldspar, albite, chlorite, and pyrite,
218 developed in the host rocks (Fatyanov and Khomich, 1989). Lateral zoning also occurs
219 in the skarn-like Mg-Fe alteration zone developed in dolomites near their contact with the
220 hydrothermally altered andesitic tuffs, with a zonation of serpentine, tremolite, diopside,
221 and actinolite-epidote facies as the tuffs are approached. The first three formed in
222 dolomites, whereas the fourth occurs in the andesitic tuffs.

223 At shallower levels along the vein and alteration halo, the carbonate unit shows a
224 marked change in composition. In the partly eroded Glavnaya zone, representing the lower
225 levels of mineralization, the preserved fragments of carbonate bodies are represented by
226 dolomite, whereas in the less eroded Promezhutochnaya zone this is represented by
227 calcite, usually Mn-bearing. The skarn mineralogy is governed by the matrix composition:
228 with Mg-Fe skarn is developed on dolomites, Mn-skarn forms from Mn-bearing calcites,
229 and Fe skarn in the quartz-rich zones.

230 The main ore mineralization of the deposit is also vertically zoned. At deep levels in
231 ore zones, a gold-sulfosalt-sulfide association occurs (Au-Ag – 1:0.5 to 13.6), which

changes at shallower levels to gold-sulfide ore (Au:Ag – >1:0.5), thereafter to gold-telluride-sulfide association (Au:Ag – 1:0.5 to 3), and finally to telluride-sulfide (Au:Ag – 1:3-1:10) (Fatyanov et al., 2007), Fig. 13. Thus, the Mnogovershinnoe deposit is a good example of vertical zoning of gold-silver mineralization.

6. Discussion

The diversity of geological settings in which the epithermal precious metal deposits are formed has been addressed in various studies (Fatyanov, 1980; Goncharov, 1982; Petrenko, 1999; Konstantinov at al., 2000; Cox, 2005; Simmons et al., 2005; Fatyanov et al., 2009; Fig. 14. The formation of the Mnogovershinnoe deposit has been evaluated based on an analysis of available information on structure and geophysical data on the veins and alteration halos (Bondarenko, 1977; Konstantinov at al., 2000; Khomich at al., 2004; Vartanyan and Novikov, 2015). Here we address the main stages of the deposit formation based on the model presented in Fig. 15.

We envisage that the formation of the Bekchiul volcano-plutonic complex was related to heat input into the upper domains of the mantle from the dehydrating stagnant oceanic slab in the mantle transitional zone (Fig. 15A).

The emergence of a peripheral magmatic chamber at hypabyssal level and the formation of volcanic regime (the earliest manifestation of which is dated as Late Cretaceous (85-78.5 Ma; Bondarenko, 1977) resulted in the reconstruction of the hydrothermal system surrounding the volcano-plutonic complex. The early stage of the fluid system during the development of the andesite-granodiorite correlates with the magma chamber of the volcanic center, followed which was later replaced by meteoric regime. The processes of voluminous metasomatic transformation (propylitization, in particular) continued until equilibrium of the fluid-rock system was attained (propylitized

andesites are dated as 81-76 Ma; Bondarenko, 1977). Along the linear steeply dipping tectonically weakened structures, which served then the channels for the fluid filtration, intensive leaching occurred with the formation of the metasomatic zone characterized by sericite-quartz (Fig. 15B). The age of the quartz-sericite zone is dated as 76-65 Ma (Konstantinov et al., 2000).

The volcano-plutonic complex at the center formed a dome-like edifice. Stress propagation along both the earlier emplaced tectonic dislocations and orthogonal (across the strike of the former) faults with large fault-shift displacements occurred. The dislocation fractures were almost synchronously healed with quartz-veins. The major stage of mineral deposition resulted in the formation of mineral “plugs” and increase of fluid pressure at the regions of fluids ponding, leading to explosive brecciation and cementation of fragments with quartz, adularia-quartz, and in some cases carbonate-quartz aggregates. This may suggest a stable tectonic setting during the development of ore, with extension of localizing structures through the domal uplift of the Bekchiul volcano-plutonic center (Fatyanov et al., 2010). In vast the aureoles around the brecciation zones, the streaky recrystallization of the earlier formed hydrothermal components occurred with the development of breccia-like streaky megastructures (Fig. 15C). The adularia-quartz zones are dated as 75,4-66,4 Ma (Khomich et al., 2004), Table 1.

Gradual exhaustion of the source of the magmatic fluids led to the fluid pressure decrease in the hydrothermal system to the levels providing again the connection to the drainage channels of infiltration from the pore spaces surrounding the rocks. The formation in some areas of ore-localizing structures of small carbonate bodies is related with this stage of filtration (Fig. 15D).

During the culmination of the hydrothermal activity, the system was replenished by the near-neutral fluids (Fig. 15E). However, the late stage intrusion of magmas that generated the monzogranodiorite-granite association resulted in heating of the

surrounding rocks (the monzogranodiorites are dated as 66.4-57,3 Ma (Khomich et al., 2004), Table 1. The carbonate component of the earlier zones underwent skarnization. The skarn-like associations were developed locally and on the quartz filling of zones. In the contact aureole of monzogranodiorites, the vein-metasomatic zones were recrystallized. Cooling to temperatures of the pre-skarn period caused the resumption of the carbonate deposition. The post-skarn carbonate bodies mark the final completion of the activity of the hydrothermal system responsible for the formation of the mineralized vein-metasomatic zones of the deposit (Fig. 15F).

The development of a new hydrothermal system and formation of the tourmaline-quartz vein-streaky series is related with the intrusion of subalkaline granitoid magmas (monzodiorite-granite association of the volcano-pluton – 66.4-57,3 Ma (Khomich et al., 2004), Table 1.

The hydrothermal system of Mnogovershinnoe deposit is considered to be polygenic. At the early stage, the system was fed from the peripheral part of the volcano-plutonic complex. At the waning stage of the magmatic system, the fluids mixed with those of meteoric origin (Fatyanov et al., 2009).

The heated meteoric waters penetrated into the hydrothermal system, when the fluid pressure decreased allowing the convective cell to percolate within the pore spaces of the surrounding rocks. The hydrothermal activity and ore deposit formation are shown in a schematic illustration in Fig. 14. The dynamic scheme also demonstrates the possibility of both synchronous and successive development of the structures and mineral deposit (Fig. 15A-F).

7. Conclusion

1. The formation of the Mnogovershinnoe gold-silver deposit is related with the hydrothermal activity of the Bekchiul volcano-plutonic complex in the Late Cretaceous-Paleogene time.

2. Steeply dipping rupture dislocations, inherited from the deformation of the Jurassic-Cretaceous basement, functioned as the main ore-localizing structures. They enclose thick alteration zones (to 100 m) and long veins (to 5-7 km) with precious-metal mineralization in the volcanic host and its terrigenous basement for several hundred meters vertically.

3. Ore-bearing zones show a complex structure. The various zones recognized are: metasomatic zone of acid leaching, quartz-vein and carbonate filling, skarn-like metasomatic bodes, contact-metamorphosed substratum, and tourmaline-quartz vein-streaky series. Among these, the quartz-vein filling and their vast cover of the hydrothermally altered rocks are the major zones.

4. The development of ore-bearing zones is governed by the hydrothermal activity accompanying the emplacement of the Bekchiul volcano-plutonic complex and interaction with meteoric waters. The Mnogovershinnoe deposit provides a case for polychronous ore-forming systems.

Acknowledgments

We thank Editor-in-Chief Prof. Franco Pirajno and Referees J. Hedenquist and Andy Wilde for constructive comments. This work was carried out with the financial support of the Presidium and Far East Branch of the Russian Academy of Sciences (№ 15-I-2-019). Valentina Piskunova and Inessa Strel'chenko are thanked for their help with the work.

335 **References**

336

337 Bondarenko, E.I., 1977. Evolution of Mesozoic-Cenozoic magmatism and mineralization of
338 the northern part of the Sikhote-Alin folded system according to radiological
339 data. Extended abstract of doctoral (geol.-miner.) dissertation, Dal'nauka,
340 Vladivostok, pp. 1-31 (in Russian).
341 Cox, S.F., 2005. Coupling between deformation, fluid pressures and fluid flow in ore-
342 producing hydrothermal systems at depth in the crust. In: Economic Geology
343 100th Anniversary volume. Society of Economic Geologists, pp. 39-76.
344 Didenko, A.I., Malyshev, Yu.F., Saksin, B.G., 2010. Deep structure and metallogeny of
345 East Asia. Dal'nauka, Vladivostok, pp. 1-232 (in Russian).
346 Fafyanov, I.I., 1980. Stages and temperature conditions of formation at one of the gold
347 deposits of the Lower Amur region. Thermobarogeochemistry and ore
348 genesis. DVO AN SSSR, Vladivostok, pp. 162-169 (in Russian).
349 Fatyanov, I.I., Khomich, V.G., 1989. The structure and features of the formation vein-
350 metasomatic zones of gold-silver deposit East Sikhote-Alin volcanic belt. In:
351 Geological conditions of localization of endogenous mineralization. DVO AN
352 SSSR, Vladivostok, pp. 86-100 (in Russian).
353 Fatyanov, I.I., Khomich, V.G., 1997. Bekchiul gold-bearing volcano-plutonic construction:
354 magmatic associations, features of development, the scheme of formation
355 (Lower Amur region). Tikhookeanskaya geologiya 16, 32-44 (in Russian).
356 Fatyanov, I.I., Khomich, V.G., 2001. Structural and material elements of vein-metasomatic
357 zones of Mnogovershinnoe gold-silver deposit (Lower Amur region) as
358 indicators of the evolution of hydrothermal ore-forming system. Ore deposits of
359 continental margins. Iss. 2. Part 2. Dal'nauka, Vladivostok, 322-331 (in
360 Russian).

361 Fatyanov, I.I., Khomich, V.G., Boriskina, N.G., 2007. Non-traditional method of typification of
362 ores of gold-silver deposits (on the example of the Mnogovershinnoe deposit,
363 Lower Amur region). Vestnik Tomskogo gosudarstvennogo 304, 211-217 (in
364 Russian).
365 Fatyanov, I.I., Khomich, V.G., Boriskina, N.G., 2009. Reconstruction of the ore-forming system
366 in the Mnogovershinnoe gold-silver deposit (Lower Amur River Region) based
367 on the structure of ore-bearing zones and isotopic studies. Russian Journal of
368 Pacific Geology 3, 19-27 DOI: 10.1134/S1819714009010035
369 Fatyanov, I.I., Khomich, V.G., Boriskina, N.G., 2010. Hidden mineralogical and geochemical
370 zonation of low-sulfide gold—silver mineralization (Mnogovershinnoe deposit,
371 Lower Amur area). Doklady Earth Sciences 435, 1456-1459 DOI:
372 10.1134/S1028334X10110103
373 Fatyanov, I.I., Sapin, V.I., 1988. Selenium mineralization at one of the gold-silver deposits
374 of the Lower Amur region. Geologiya rudnykh mestorozhdeniy 30, 110-114
375 (in Russian).
376 Fatyanov, I.I., Yas'kin, G.M., Valui, G.A., 1989. Adularia at one of the gold-silver deposits of
377 the Lower Amur region and features of its the formation. Tikhookeanskaya
378 geologiya 1, 108-112 (in Russian).
379 Goncharov, V.I., 1982. Model of hydrothermal ore-forming systems Okhotsk-Chukotka
380 volcanic belt. In: Materials on Geology and Mineral Resources of the North-
381 East of the USSR. SVKNII, Magadan, iss. 26, pp. 121-126 (in Russian).
382 Khanchuk, A.I., 1993. Geological structure and development of the continental framing of
383 northwest Pacific. Extended abstract of doctoral (geol.-miner.) dissertation. GIN
384 RAN, Moscow, pp. 1-31 (in Russian).

385 Khomich, V.G., Boriskina, N.G., 2014 a. Localization of PGE mineralization in southeastern
386 Russia. Russian Geology and Geophysics 55, 842-853.
387 DOI:10.1016/j.rgg.2014.06.004
388 Khomich, V.G., Boriskina, N.G., 2014 b. Geodinamic settings of formation of large deposits of
389 precious and radioactive elements in Inagli-Konder-Feklistov belt and its flanks.
390 Gelolgy and mineral resources of Siberia 3s-1, 37-40 (in Russian).
391 Khomich, V.G., Boriskina, N.G., Santosh, M., 2014. A geodynamic perspective of world-
392 class gold deposits in East Asia. Gondwana Research 26, 816-833. DOI:
393 10.1016/j.gr.2014.05.007
394 Khomich, V.G., Boriskina, N.G., Santosh, M., 2015. Geodynamics of late Mesozoic PGE,
395 Au, and U mineralization in the Aldan shield, North Asian Craton. Ore
396 Geology Reviews 68, 30-42. DOI:10.1016/j.oregeorev.2015.01.007
397 Khomich, V.G., Fatyanov, I.I., Lebedev, V.A., Boriskina, N.G., Ignatyev, A.V., 2004.
398 Geochronology of the formation of the Bekchiul gold-bearing volcano-plutonic
399 construction (Lower Amur region) // In: Materials of XVII Symposium on isotope
400 geochemistry. IGEM, Mascow, pp. 270-271 (in Russian).
401 Khomich, V.G., Petrishchevskiy, A.M., 2004. Protomagmatie chambers of the Near-Amur
402 gold-bearing systems. Vulkanologiya i seismologiya 1, 25-38 (in Russian).
403 Konstantinov, M.M., 2010. Gold deposits of Russia. Aquarel, Moscow, pp. 1-349 (in
404 Russian).
405 Konstantinov, M.M., Vargunina, N.P., Kosovez, T.N., Struzhkov, S.F., Syngaevskiy, E.D.,
406 Shishakova, L.N., 2000. Gold-silver deposits. In: Models deposits of precious
407 and non-ferrous metals. TSNIGRI, Moscow, pp. 1-239 (in Russian).
408 Krasnyi, L.I., Peng Yungbiao, 1998. Geological map of the Amur region and adjacent
409 areas. Scale 1: 12500000. Fabrika VSEGEI, St.Peterburg (in Russian).

Li, C., van der Hilst, R. D., 2010. Structure of the upper mantle and transition zone beneath Southeast Asia from traveltime tomography. J. Geophys. Res. 115. B07308, DOI: 10.1029/2009JB006882.

Maruyama, S., Santosh, M., Zhao, D., 2007. Superplume, supercontinent, and post-perovskite: Mantle dynamics and antiplate tectonics on the Core-Mantle Boundary. Gondwana Research 11, 7-37. http://dx.doi.org/10.1016/j.gr.2006.06.003.

Petrenko, I.D., 1999. Gold-silver formation of Kamchatka. Petropavlovsk-Kamchatsky. VSEGEI, St. Petersburg, pp. 1-116 (in Russian).

Petrishevsky, A.M., 1988. Statistical gravitational model of the lithosphere of the Far East. DVGU, Vladivostok, pp. 1-168 (in Russian).

Petrishevsky, A.M., Yushmanov, Yu.P., 2014. Correlation between ore deposits of the Lower Amur river region with the deep structures of the Earth's crust. Doklady Earth Sciences 457, 1014-1019. DOI: 10.1134/S1028334X14080157

Simmons, S.F., White, N.C., John, D.A., 2005. Geological characteristics of epithermal precious and base metal deposits. In: Economic Geology 100th Anniversary volume. Society of Economic Geologists, pp. 485-522.

Utkin, V.P., 1999. Horst-accretionary systems, rift-grabens and volcano-plutonic belts of the Russian Far East south. Paper 2. Volcano-plutonic belts: structural-compositional characteristics and regularities of formation. Russian Journal of Pacific Geology 14, 891-922.

Vartanyan, S.S., Novikov, V.P., 2015. Gold-silver deposits of the volcano-plutonic belts. Rudy i metally 1, 14-29 (in Russian).

Yushmanov, Yu.P., 2014. Structural-tectonic patterns of gold distribution in the Pilda-Limuriysky ore district, Lower Priamurie. Tikhookeanskaya geologiya 33, 99-109 (in Russian).

436 Zhao, D., Pirajno, F., Dobretsov, N.L., Liu, L., 2010. Mantle structure and dynamics under
437 East Russia and adjacent regions. Russian Geology and Geophysics 51,
438 925-938. DOI: 10.1016/j.rgg.2010.08.003.
439 Zorin, Yu.A., Turutanov, E.H., Kozhevnikov, V.M., Rasskazov, S.V., Ivanov, A.V, 2006. On
440 the origin of Cenozoic upper mantle plumes in East Siberia, Russia and in
441 central Mongolia. Geologiya i Geofizika 47, 1060-1074 (in Russian).
442
443

444 **Figure captions**

445

446 **Fig. 1.** Schematic geological map of southeast Russia, along the coast of the
447 Okhotsk Sea. Modified after Krasnyi and Peng (1998).

448 **Fig. 2.** A) Part of the Asia-Pacific zone of convergence, showing the longitudinal
449 seismic wave velocities; B) location of giant gold deposits in East Asia with respect to the
450 of deep-seated tectonic divisions; C) density distribution (1 unit = 10^{-2}kg/(m^2·km). Z_0=31-50
451 km depth, marking the centers of density inhomogeneities, Hc=30 is the depth of the
452 surface to which density inhomogeneities of the layer is condensed. Figures compiled after
453 data in Zorin et al. (2006), Zhao et al. (2010), Khomich et al. (2014), Khomich and
454 Boriskina (2014 b), and Petrishevsky and Yushmanov (2014), with additions.

455 **Fig. 3.** Schematic geological map of the Bekchiul volcanic-plutonic structure.

456 **Fig. 4.** Geological map and section of the Mnogovershinnoe ore field. Based on
457 geological exploration work.

458 **Fig. 5**. Section of Promezhutochnoe ore body, hor. 305 m (ad. 11).

459 **Fig. 6.** Zoning scheme of the Verkhnee ore body (Mnogovershinnoe deposit).
460 Modified after Konstantinov (2010).

461 **Fig. 7.** Typical textures of ores in the vein metasomatic zones of the
462 Mnogovershinnoe deposit. A - Striped adularia quartz ore with fragments of early fine-
463 grained quartz (Q). Ore body of Verkhnee. B - Striped adularia quartz ore with fragment of
464 siltstone (black). Ore body of Verkhnee. C-D - Wollastonite (Woll) and bustamite (Bust)
465 substitutes carbonates (Carb). Sphalerite and galena is confined to the contact and
466 distributed along margins. Ore zone of Promezhutochnaya. E - Sulfide pyrite chalcopyrite
467 ore. Ore body Severnoe. F - Fragment of the striped adularia quartz ore in the dike of
468 basalt porphyrite (Porph). Ore body Verkhnee.

Fig. 8. Relationship between different stages of mineral formation in the Mnogovershinnoe deposit. A - Zonal magnesian-ferruginous metasomatite. Diop – diopside, Ep+Act - epidote and actinolite, Py – pyrite, Neph – nephritis, Tre – tremolite; B – Q – quartz, Tell – tellurides, Py – pyrite, Exp. brec. - explosive breccia; C - Dol - hydrothermal dolomite, Mt – magnetite; D – Bust+Rod - bustamite and rhodonite, Q – quartz; E – Q+ Bust+Rod – quartz, bustamite and rhodonite; F – Q+Woll - quartz and wollastonite.

Fig. 9. Stages and mineral associations of the Mnogovershinnoe deposit.

Fig. 10. Photomicrographs of representative minerals of ore bodies (Mnogovershinnoe deposit). A, B – fahlore; C-H – petzite (light gray) and hessite (gray) relationships; I – naumannite.

Fig. 11. Verkhnee ore body (ad. 4) in the Glavnaya ore zone (Mnogovershinnoe deposit).

Fig. 12. Gold distribution in the Verkhnee ore body (Mnogovershinnoe deposit). The projection on the vertical plane. After Konstantinov (2010) with modifications.

Fig. 13. Generalized scheme of vertical zoning in the the Mnogovershinnoe deposit.

Fig. 14. Schematic illustration showing the interaction of magmatic hydrothermal fluids and meteoric water in the convective cell leading to the formation of the mineral deposit.. After Fatyanov et al. (2009) with modifications and additions.

Fig. 15. A schematic model for the formation of the Mnogovershinnoe deposit. After Fatyanov et al. (2009) with modifications and additions.

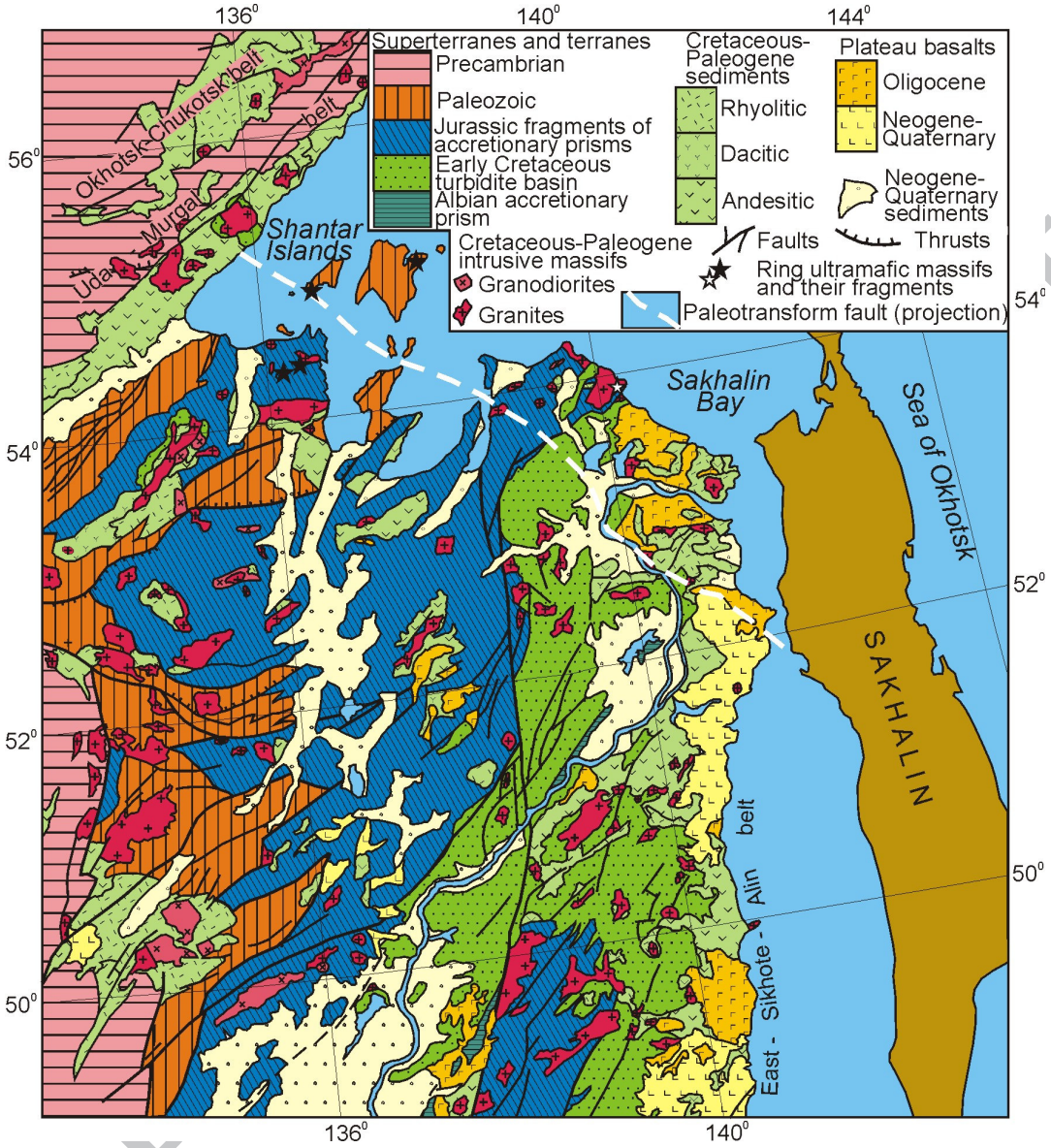
136°
140°
144°
56°
54°
52°
50°
Superterranes and terranes
Precambrian
Paleozoic
Jurassic fragments of accretionary prisms
Early Cretaceous turbidite basin
Albian accretionary prism
Cretaceous-Paleogene sediments
Rhyolitic
Dacitic
Andesitic
Plateau basalts
Oligocene
Neogene-Quaternary
Neogene-Quaternary sediments
Faults
Thrusts
Cretaceous-Paleogene intrusive massifs
Granodiorites
Granites
Ring ultramafic massifs and their fragments
Paleotransform fault (projection)
Okhotsk-Chukotsk belt
Murgal belt
Udan
Shantar Islands
Sakhalin Bay
Sea of Okhotsk
SAKHALIN
East - Sikhote - Alin belt

Fig. 1

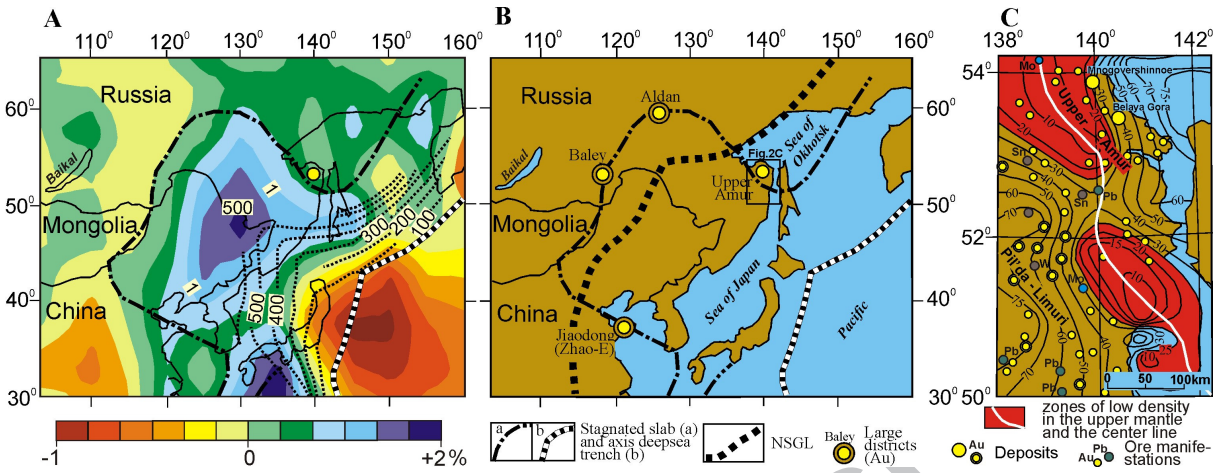

Fig. 2

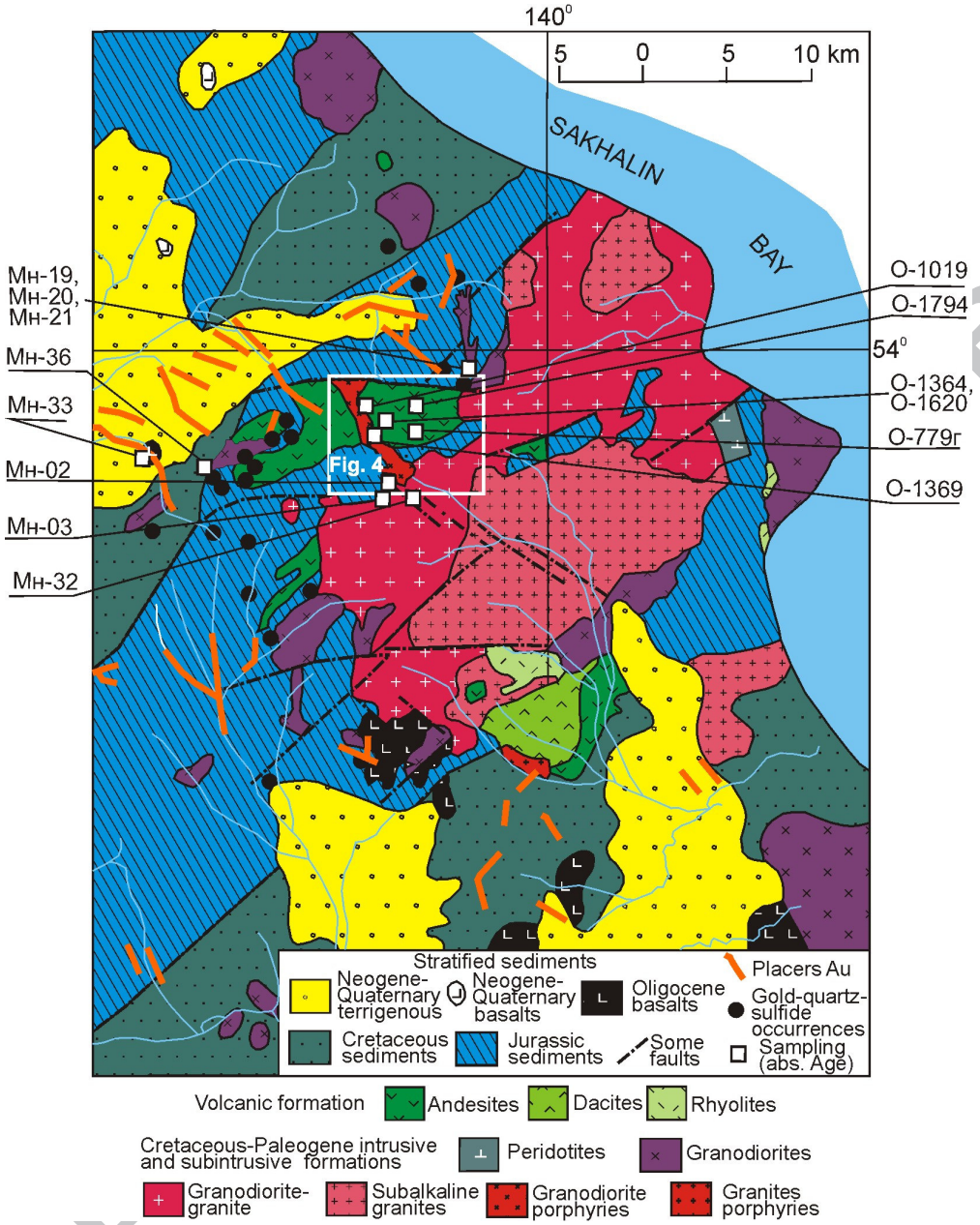

Fig. 3

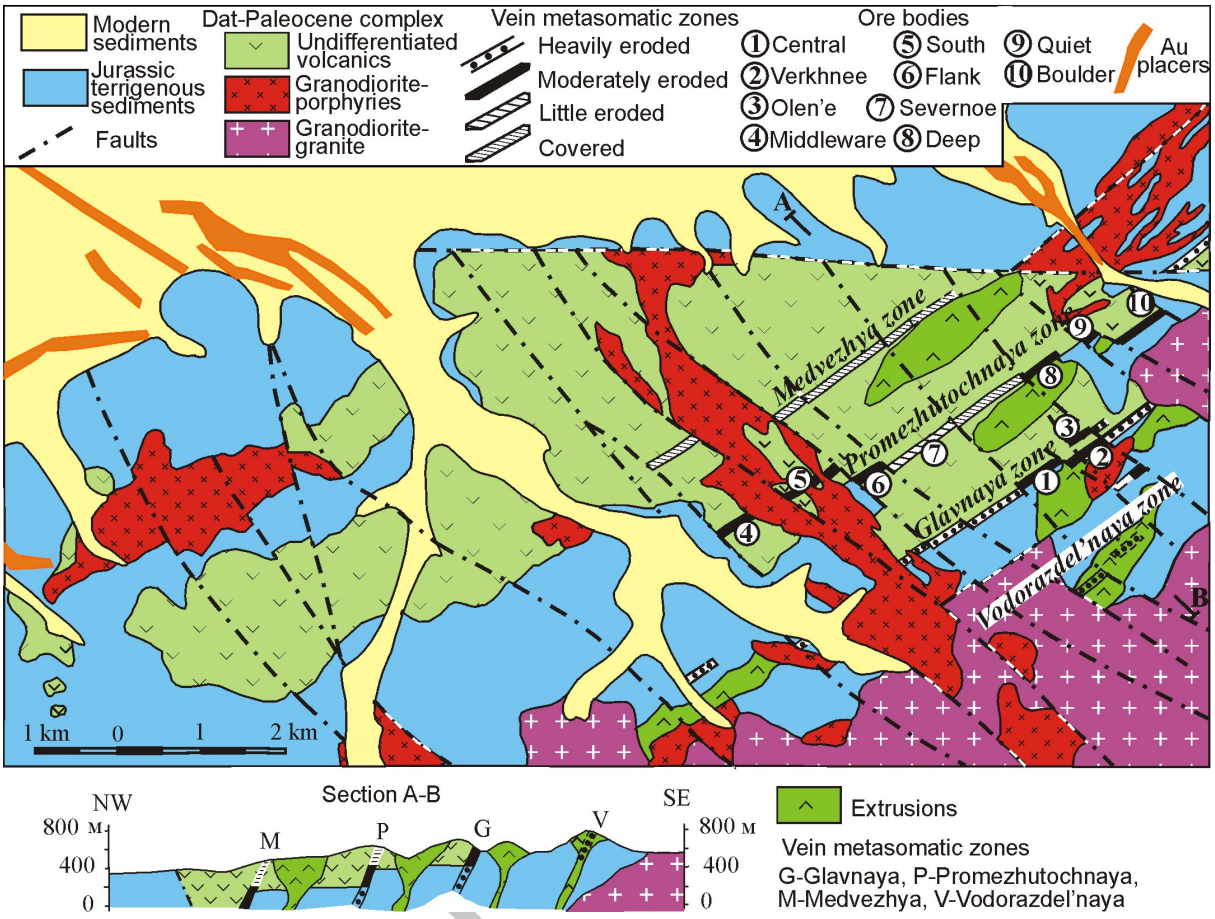

511

512

513

514 Fig. 4

515

516

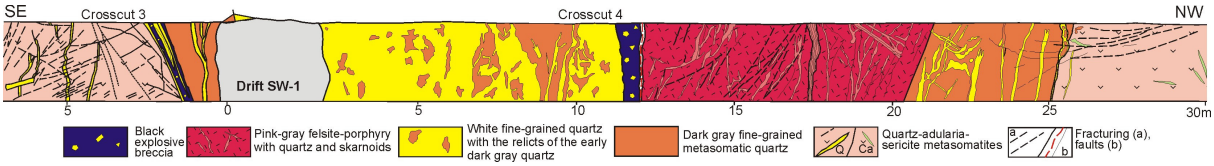

517

518

519

520 Fig. 5

521

522

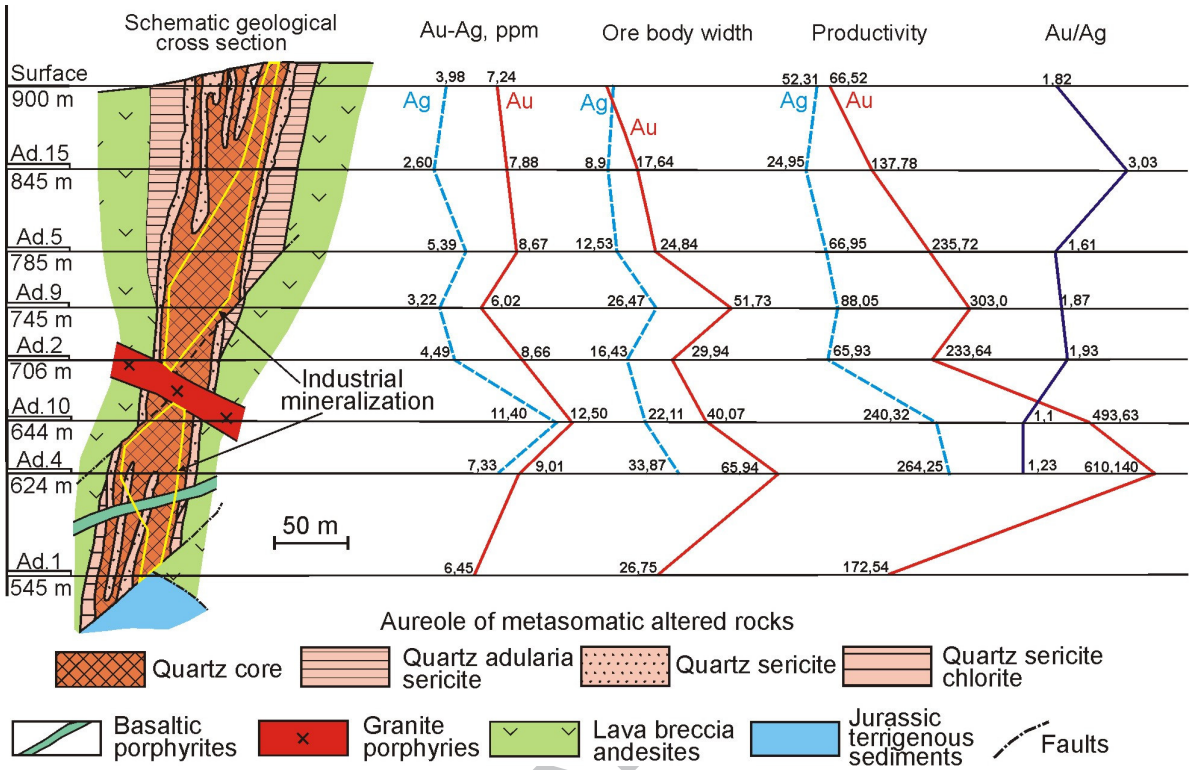

Fig. 6

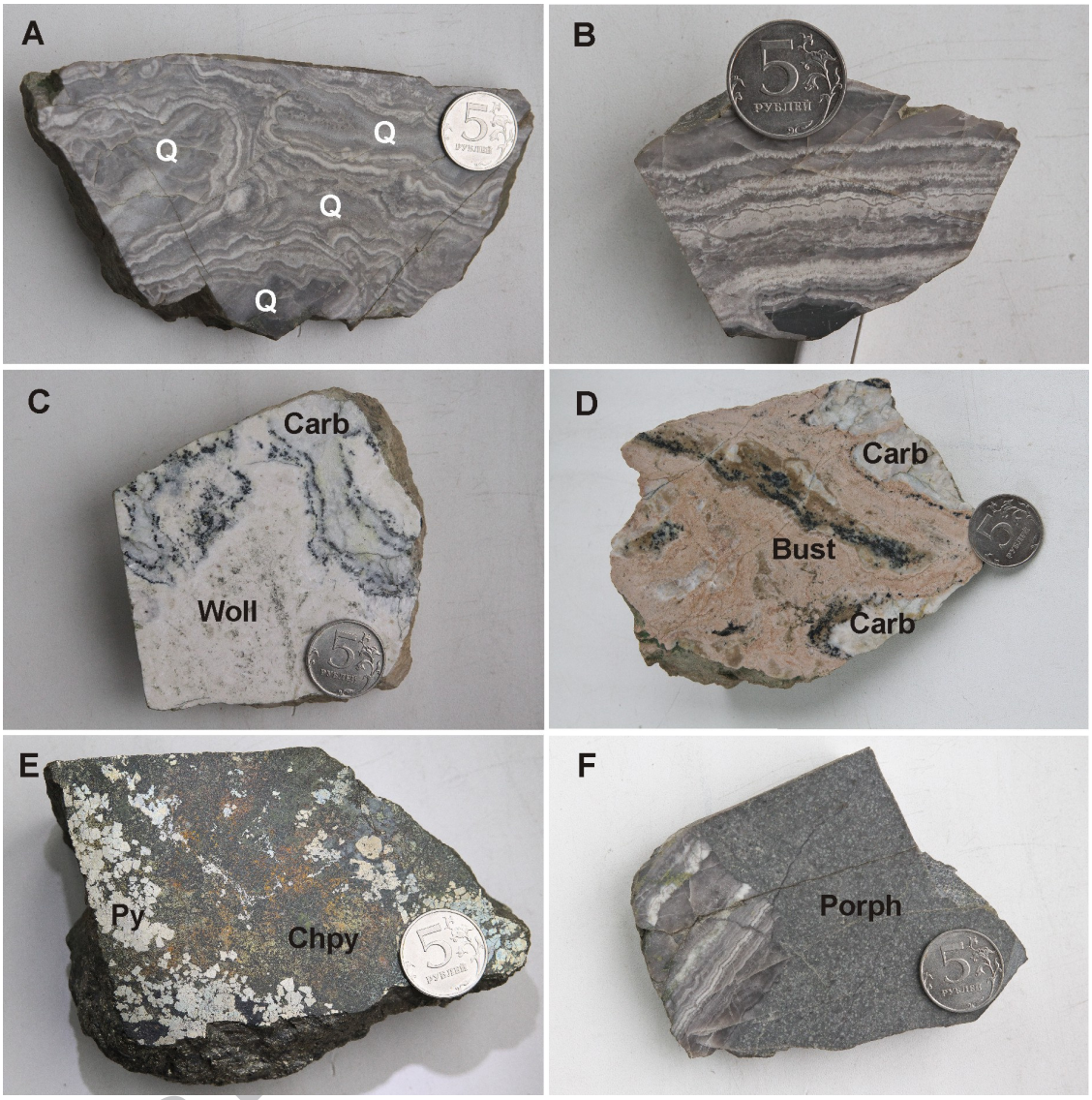

529

530

531 Fig. 7

532

533

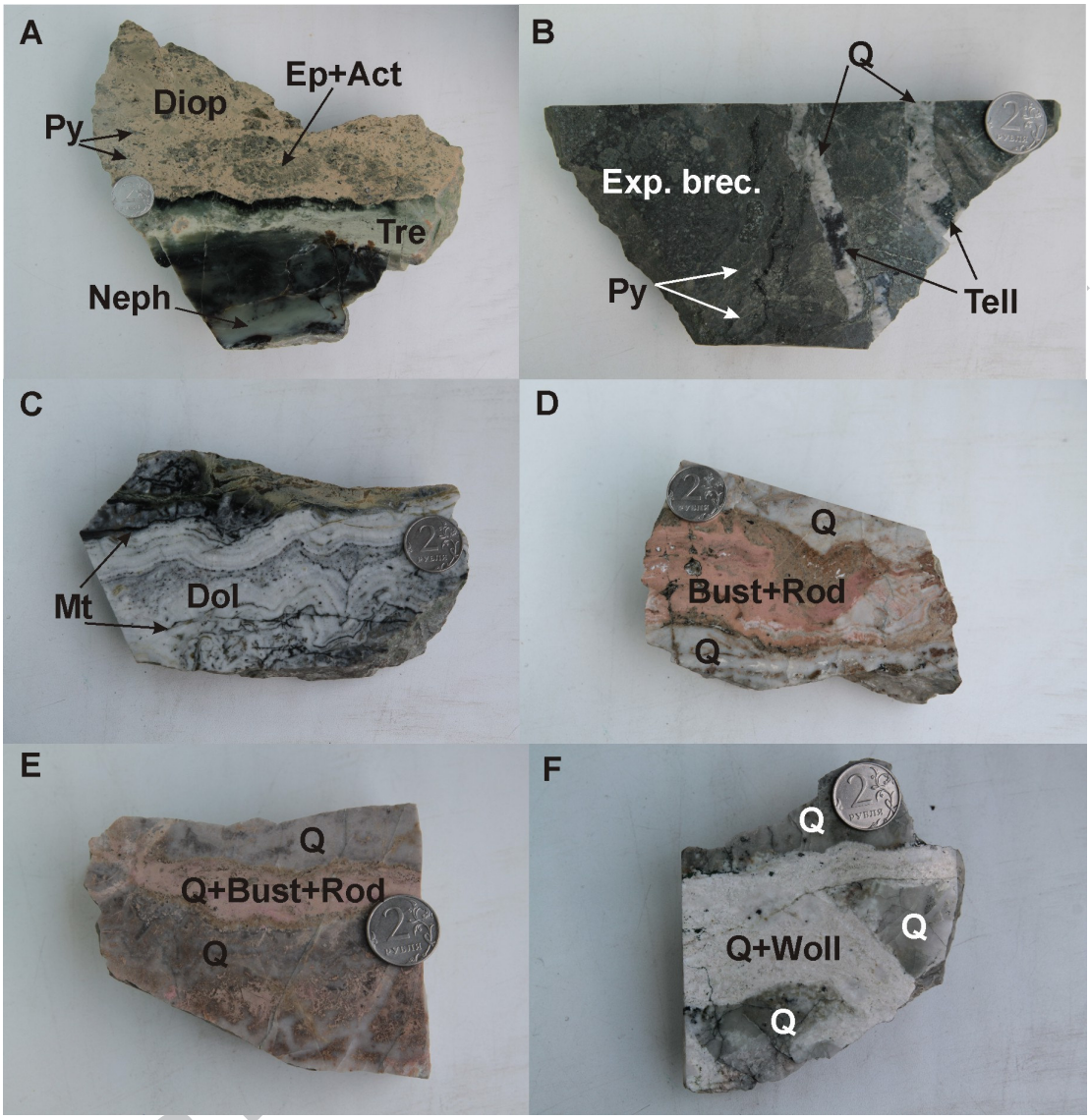

534

535

536

537 Fig. 8

538

539

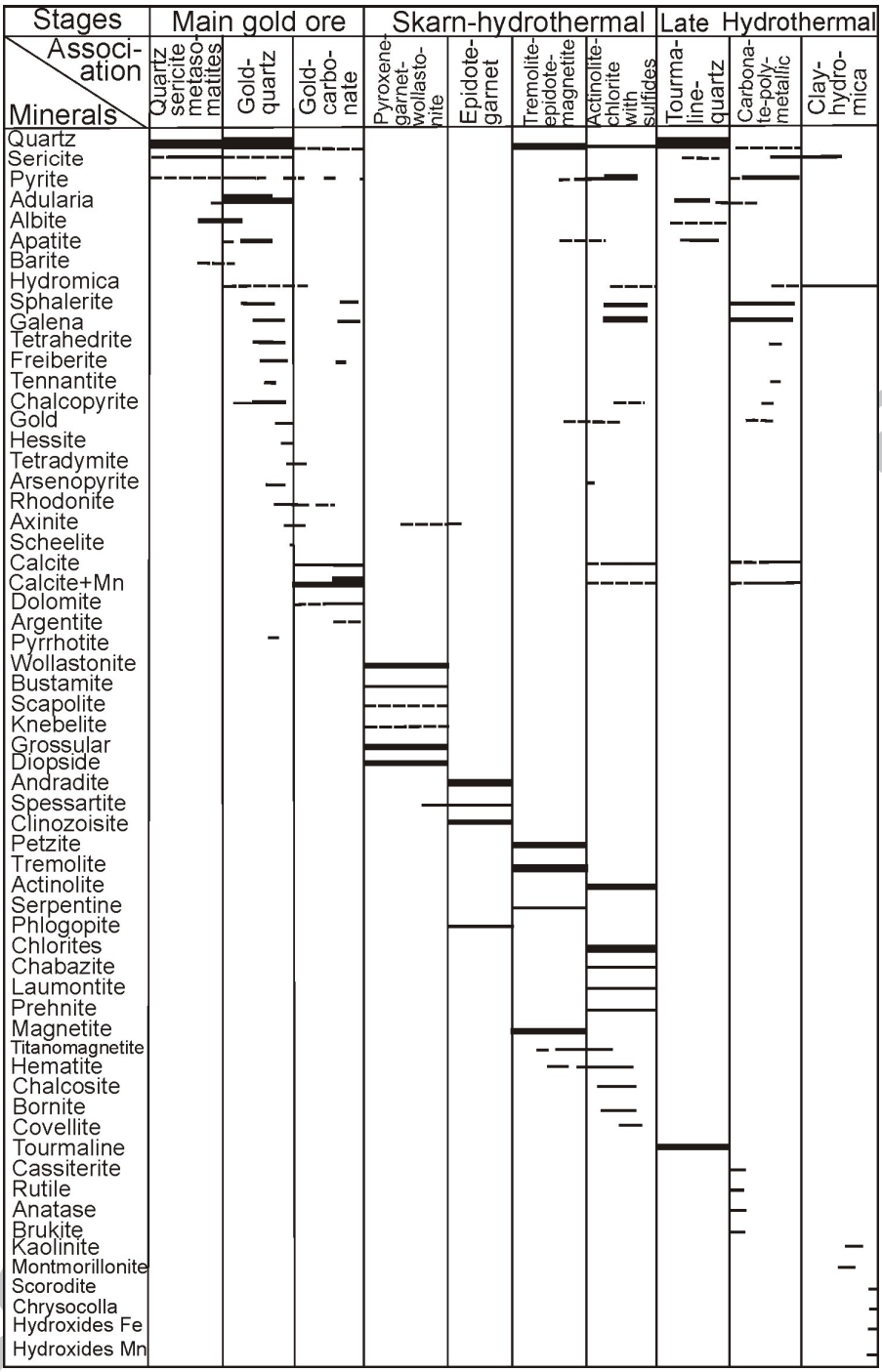

Fig. 9

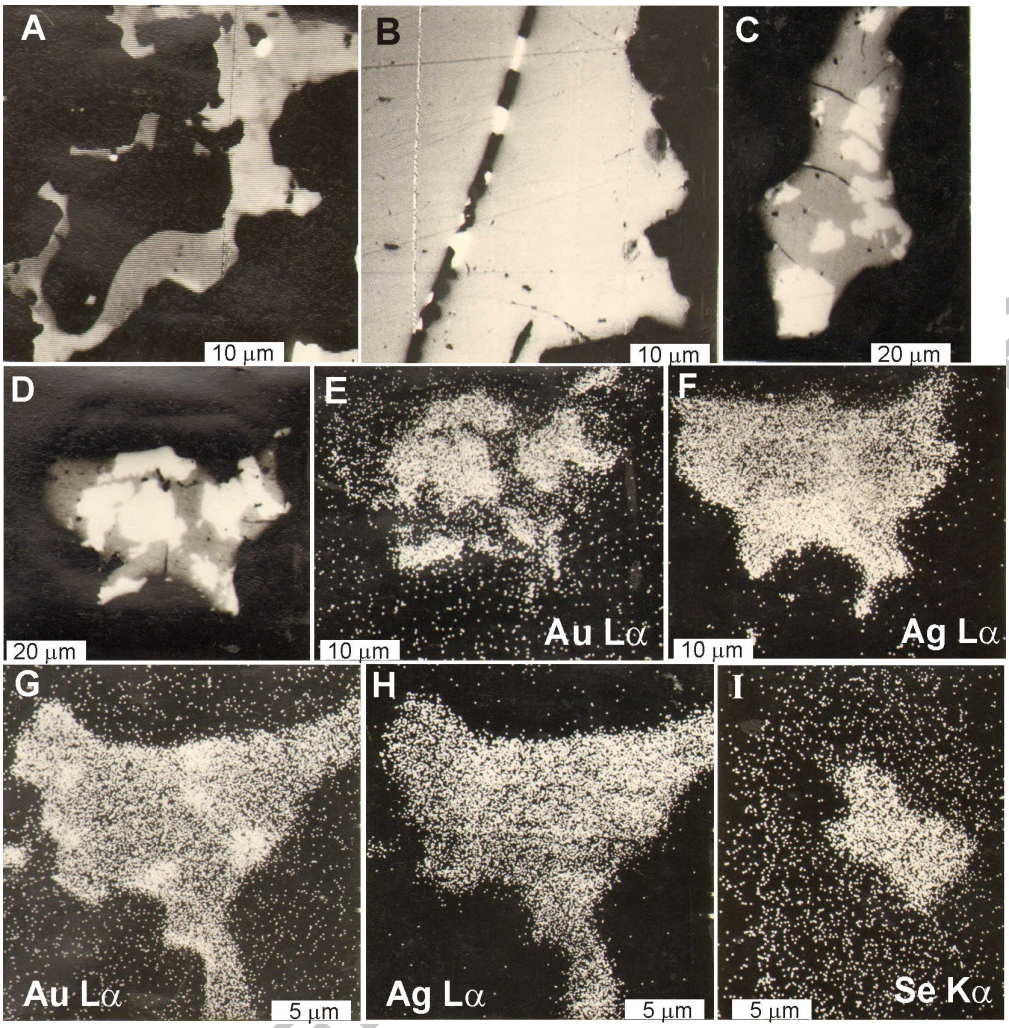

Fig. 10

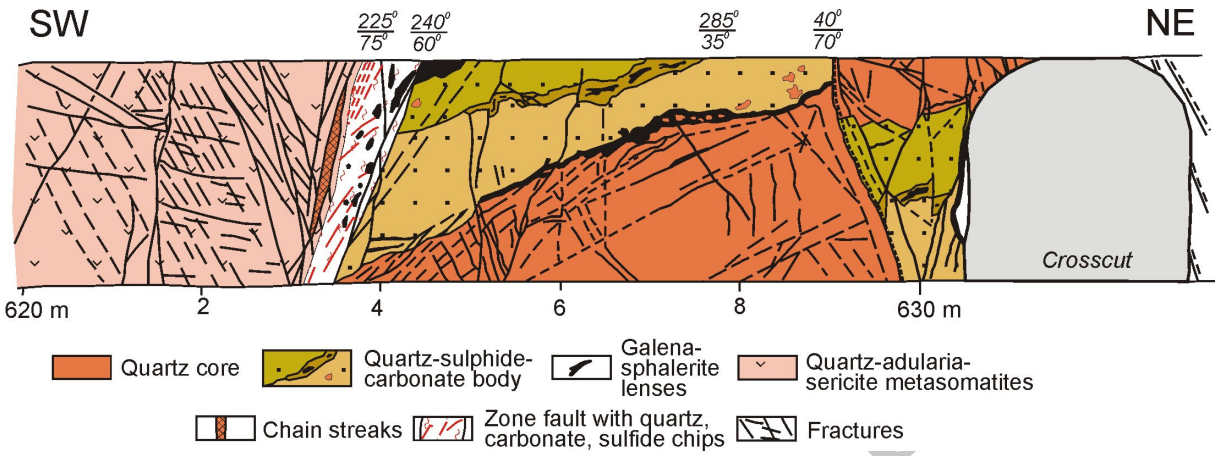

553

554

555

556 Fig. 11

557

558

559

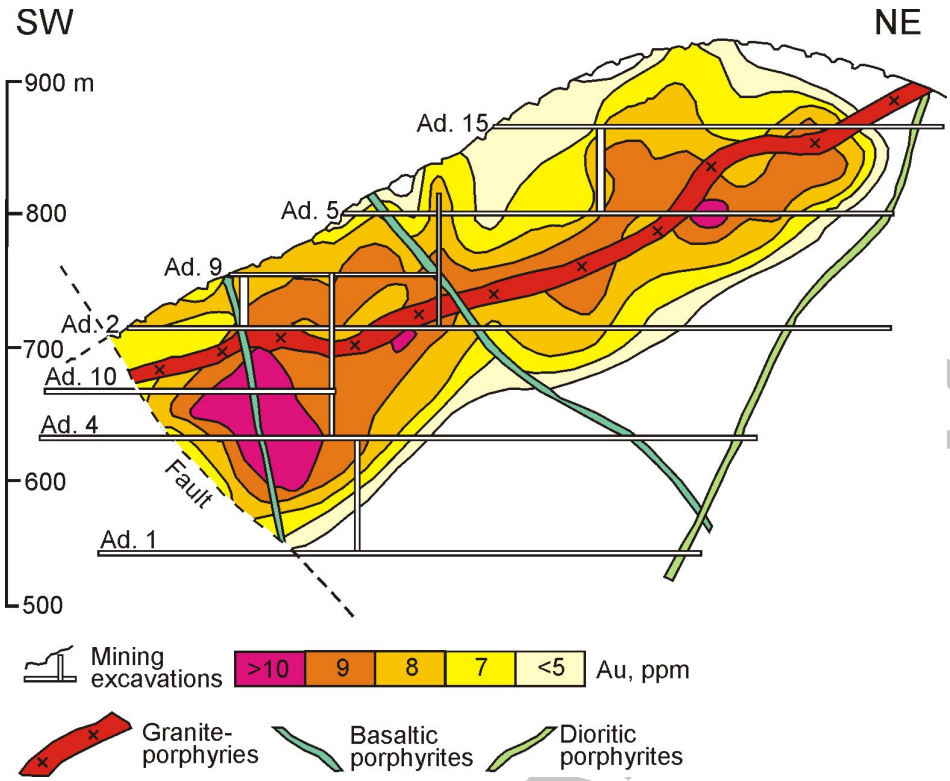

Fig. 12

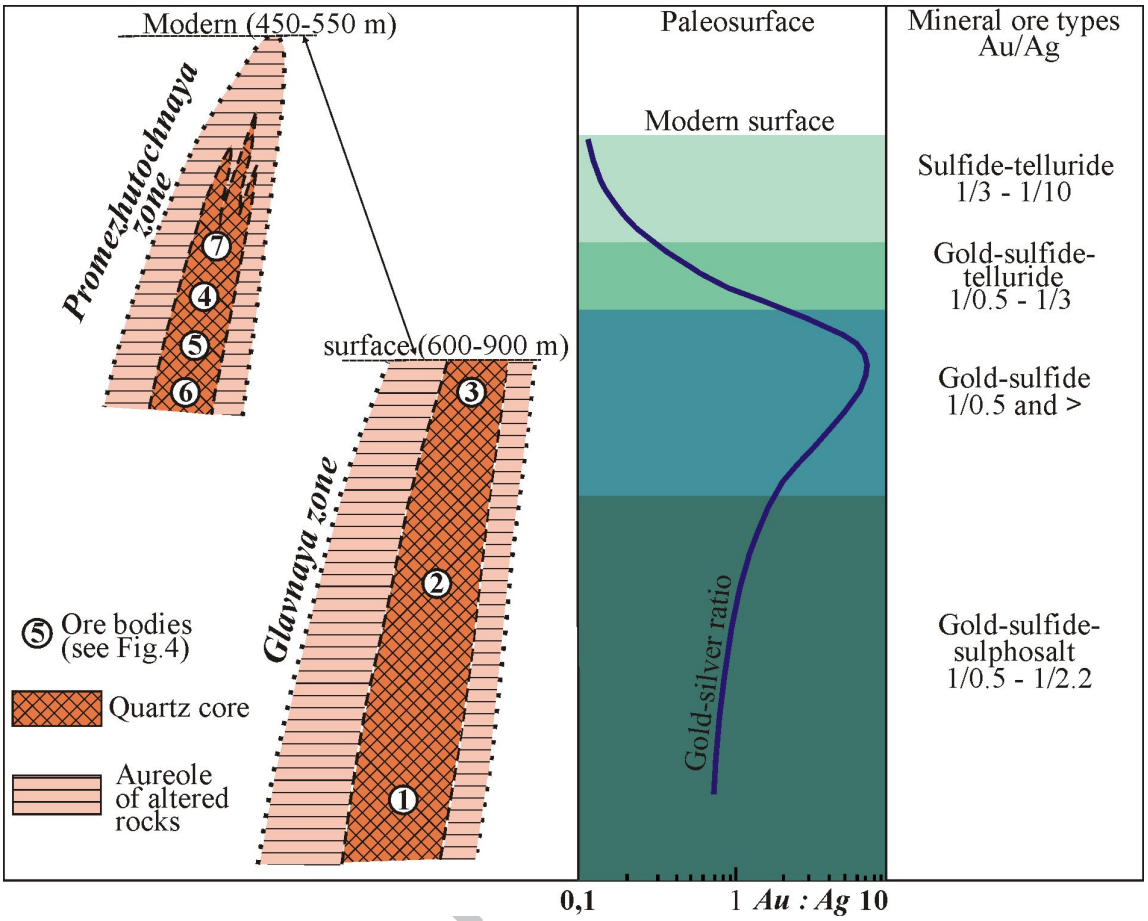

Fig. 13

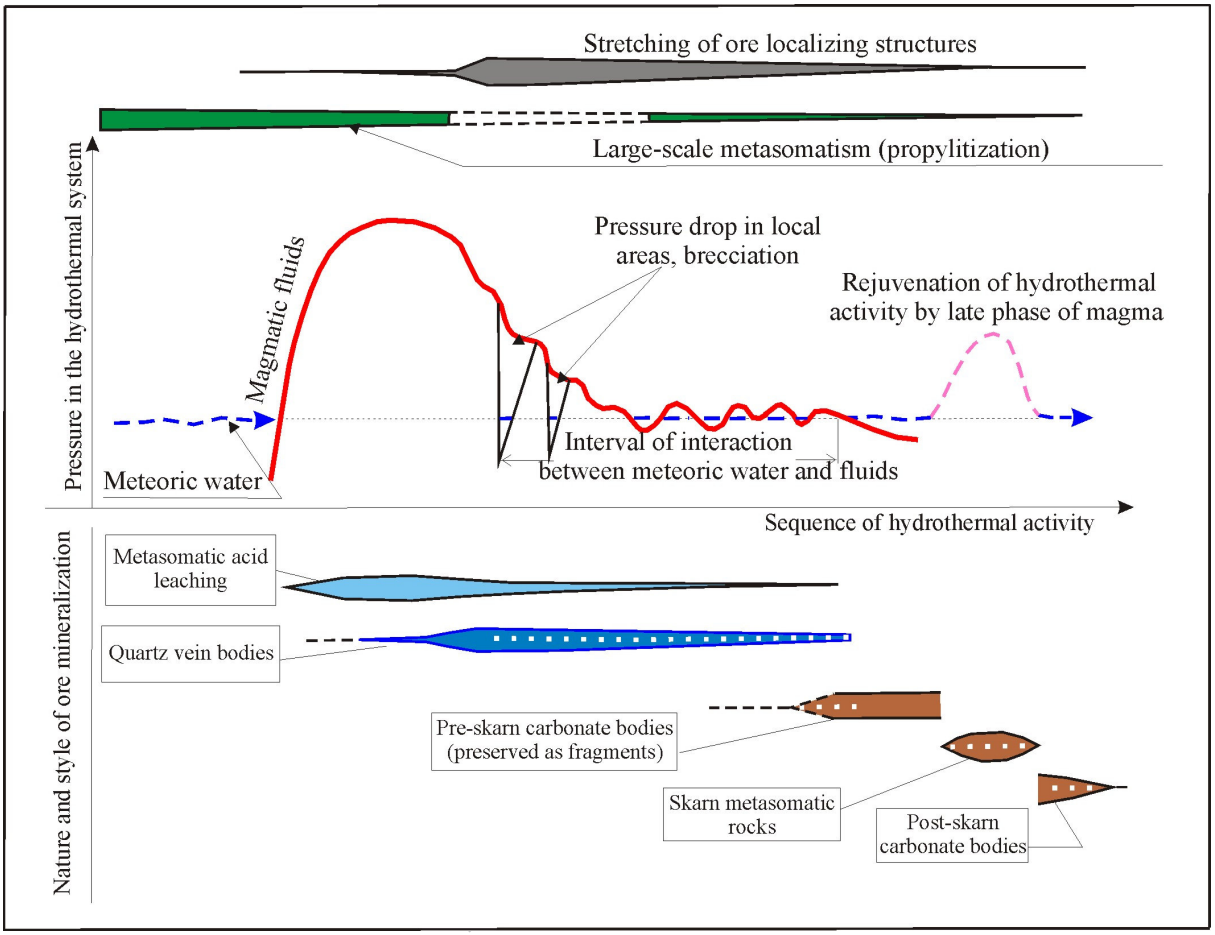

572

573

574

575 Fig. 14

576

577

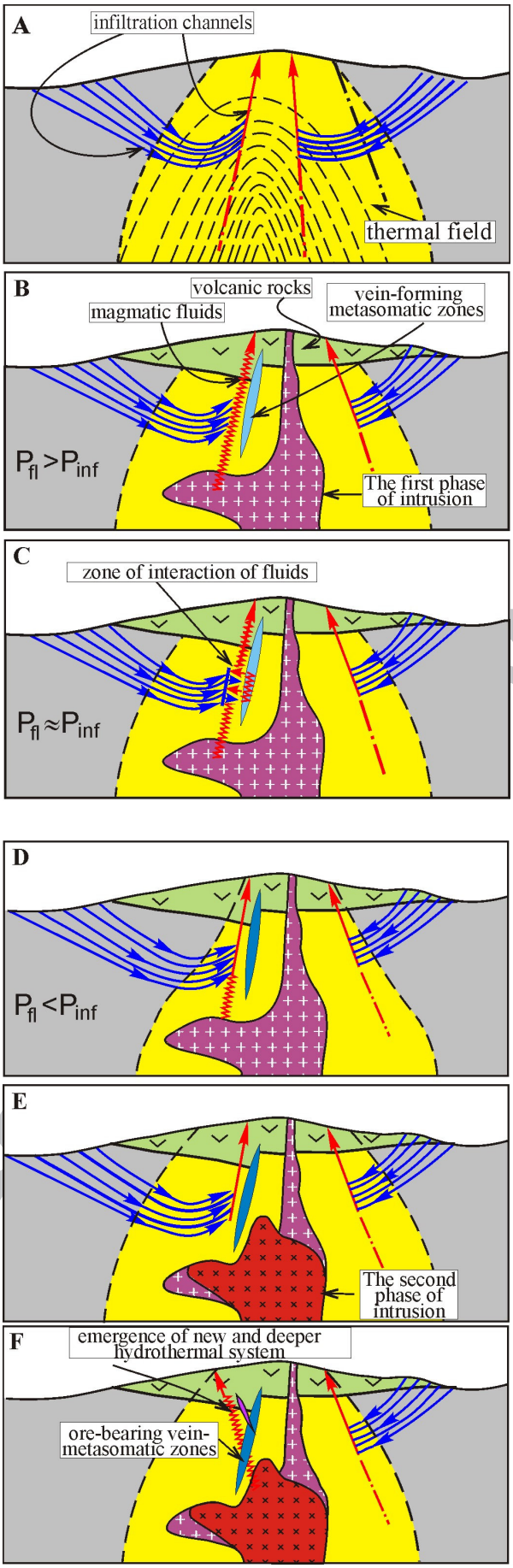

578

Table 1

The absolute age of rocks and ores in the Mnogovershinnoe ore field

Sample	Rock, mineral	Potassium, % ± σ	$^{40}Ar_{rad}$ (ppb) ± σ	Age, Ma ± 1.6σ
О-1369	**Granodiorite-porphyry: K-feldspar+ quartz**	3,34±0,05	18,3±0,6	77,1±3,2
О-779Г	Adularia,Glavnaya zone, Verkhnee body	8,97±0,07	42,4±0,8	66,9±2,4
О-1019	Adularia, Medvezhya zone	10,58±0,10	56,5±0,7	75,4±2,0
О-1364	Adularia, Promezhutochnaya zone, South and Flank body	12,61±0,12	64,2±1,2	71,9±2,4
О-1620	Adularia, Promezhutochnaya zone, South and Flank body	11,36±0,12	57,1±0,8	71,1±2,0
О-1794	Adularia, Promezhutochnaya zone, Severnoe body	12,11±0,12	56,8±0,8	66,4±1,8
Мн-02	Granodiorite-porphyry	3,98±0,04	18,2±0,6	64,9±3,0
Мн-36	Granodiorite-porphyry	3,95±0,05	21,1±0,5	75,5±3,0
Мн-21	Granodiorite	3,98±0,04	19,2±0,5	68,3±2,5
Мн-19	Andesite-dacite porphyrite	3,30±0,04	16,7±0,5	71,3±2,5
Мн-20	Andesite-dacite porphyrite	3,33±0,04	16,2±0,5	68,6±3,2
Мн-03	Monzonite diorite	3,73±0,04	15,1±0,5	57,3±3,0
Мн-32	Monzonite diorite	2,97±0,04	12,0±0,4	57,5±2,6
Мн-33	Basalt	1,96±0,03	3,35±0,15	24,5±2,0

*Radiogenic Ar abundances were measured on a specialized mass spectrometric unit at IGEM RAS using isotopic dilution with ^{38}Ar as a spike, and K abundance were measured by flame photometry. The constants used in age calculations were: $\lambda_k=0.581*10^{-10}yr.^{-1}$, $\lambda_{\beta-}=4.962*10^{-10}yr.^{-1}$, $^{40}K=0.01167$ (at. %).

590 Table 2

591 Concentration's change in the ore components of the gold-quartz stage in the

592 vertical section of the Glavnaya ore zone, weight %.

593 Based on geological exploration work.

594

Components	Horizons (abs. levels)		
	Upper (725-845 m)	Middle (625-725 m)	Lower (<625 m)
SiO_2	92,51	93,24	92,23
Al_2O_3	3,39	2,68	3,0
TiO_2	0,26	0,02	0,068
Fe_2O_3	0,79	0,90	0,70
FeO	0,95	0,93	1,20
MnO	0,07	0,08	0,064
CaO	0,68	0,47	0,58
MgO	0,392	0,82	0,30
Na_2O	0,18	0,12	0,15
K_2O	0,96	0,73	0,60
P_2O_5	0,04	0,034	0,18
Lt	0,00053	not detected	0,0009
Be	0,0003	not detected	0,00023
B	0,005	0,0026	0,0118
V	0,004	0,0014	0,0083
Cr	0,004	0,0014	0,0096
Co	0,002	0,0003	0,002
Ni	0,008	0,003	0,014
Mo	0,001	0,0006	0,0016
Ga	0,00051	0,0003	0,00072
Sn	0,0016	0,0006	0,0018
Zn	0,024	0,0008	0,001
Pb	0,0034	0,0016	0,0046
As	not detected	not detected	0,0049
Cu	0,011	0,0074	0,012
Ag, ppm	19,95	4,48	28,66
Au, ppm	9,75	6,688	97,81
Pb/Zn	0,142	2	4,6
Co/Ni	0,25	0,1	0,143

595
596

597

598

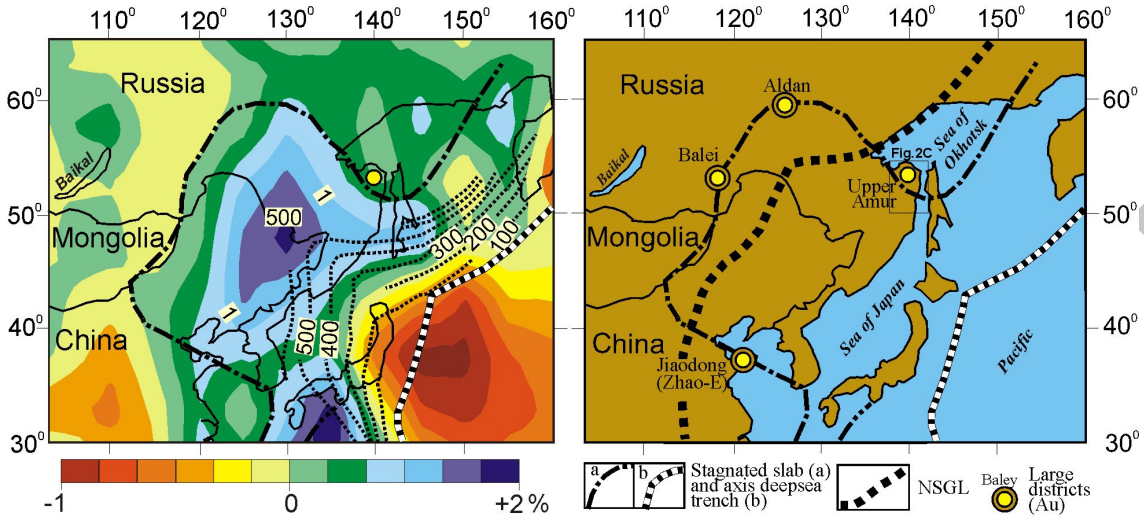

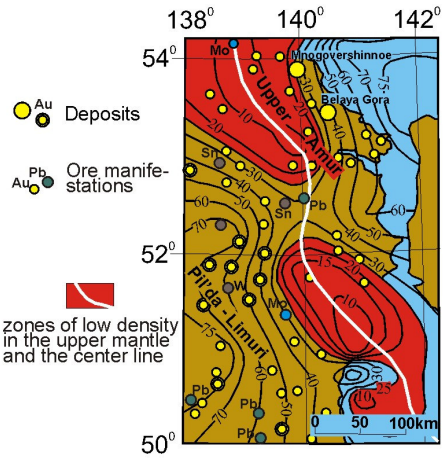

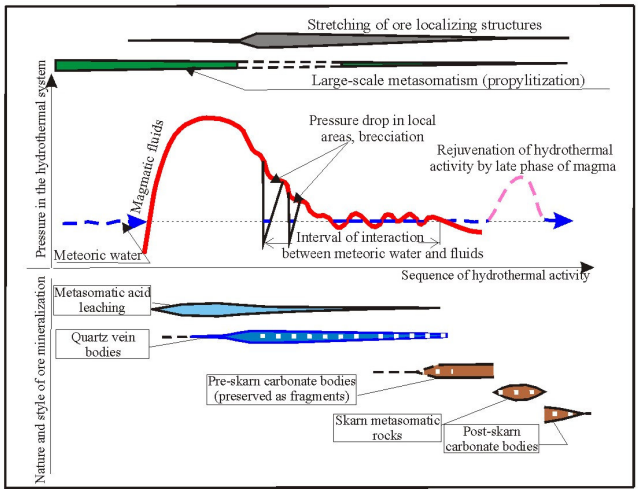

Graphical abstract